turn to the solutions for I_ν (7.3°) shown in Fig. 1 for $q = 0$ and $q = 0.002$; the observed spectrum at $\theta = 7.3°$ is superimposed.

As Fig. 1 demonstrates, the solutions for $q = 0.002$ fit the data well, whereas those for $q = 0$ show marked departures across the $S(0)$ line and smaller departures in the vicinity of the $S(1)$ line. In Fig. 6 the $q = 0$ solutions for $\Delta\tau_S$ inversely mimic the signatures corresponding in position to the $S(0)$ and $S(1)$ lines. Apparently this is how the model compensates for a lack of H_2 absorption in the troposphere in the process of fitting the limb spectrum in Fig. 1 (see also equation (5)). Conversely the $q = 0.002$ solutions for $\Delta\tau_S$ in Fig. 6 show no such inclination, implying that the H_2 opacity has been modelled correctly.

The total depth of our model atmosphere is ~90 km amagat, yielding from equation (8) a molecular hydrogen abundance of ~0.2 km amagat. This is a factor 25 lower than Trafton's[19,20] suggested value of 5 ± 3 km amagat, and a factor 10 lower than his lower limit. We cannot reconcile the two results. However, our value is consistent with the upper limit of 1 km amagat reported by Münch *et al.*[21]. It is also compatible with the steady-state mole fraction expected from balancing the production rate of H_2 (due to photochemical and charged particle decomposition of methane) with the H_2 loss rate (due to upward diffusion and subsequent blowoff at the top of the exosphere)[6].

We thank J. Pearl for helpful discussions and L. Horn and R. Koppany for observational planning; also G. L. Tyler and G. Lindal for a numerical listing for the radio occultation ingress profile, and R. Courtin for pressure-induced absorption calculations for various CH_4–N_2 mixtures in advance of publication.

Received 13 May; accepted 20 July 1981.

1. Gillett, F. C., Forrest, W. J. & Merrill, H. M. *Astrophys. J. Lett.* **184,** L93 (1973).
2. Low, F. J. & Rieke, G. H. *Astrophys. J. Lett.* **190,** L143–L145 (1974).
3. Gillett, F. C. *Astrophys. J. Lett.* **201,** L41–L43 (1975).
4. Danielson, R. E., Caldwell, J. J. & Larach, D. R. *Icarus* **20,** 437 (1973).
5. Caldwell, J. *Planetary Satellites* (ed. Burns, J.) 438 (University of Arizona Press, 1977).
6. Hunten, D. M. *NASA Conf. Publ. 2068* 127 (1978).
7. McCarthy, J. F., Pollack, J. B., Houck, J. R. & Forrest, W. J. *Astrophys. J.* **263,** 201–205 (1980).
8. Hanel, R. *et al.* Science **212,** 192–200 (1981).
9. Flasar, F. M., Samuelson, R. E. & Conrath, B. J. *Nature* **292,** 693–698 (1981).
10. Smith, B. A. *et al. Science* **212,** 163–191 (1981).
11. Tyler, G. L. *et al. Science* **212,** 201–206 (1981).
12. Savoie, R. & Fournier, R. P. *Chem. phys. Lett.* **7,** 1 (1970).
13. Obriot, J., Fondère, F., Marteau, P., Vu, H. & Kobashi, K. *Chem. phys. Lett.* **60,** 90 (1978).
14. Prydz, R. & Goodwin, R. D. *J. chem. Thermodyn.* **4,** 127–133 (1972).
15. Broadfoot, A. L. *et al. Science* **212,** 206–211 (1981).
16. Birnbaum, G. & Cohen, E. R. *Can. J. Phys.* **54,** 593–602 (1976).
17. Kiss, Z. J. & Welsh, H. L. *Can. J. Phys.* **37,** 1249–1259 (1959).
18. Kiss, Z. J., Gush, H. P. & Welsh, H. L. *Can. J. Phys.* **37,** 362–376 (1959).
19. Trafton, L. *Astrophys. J.* **175,** 285–293 (1972).
20. Trafton, L. *Icarus* **24,** 443–453 (1975).
21. Münch, G., Trauger, J. T. & Roesler, F. L. *Astrophys. J.* **216,** 963–966 (1977).

Titan's atmosphere: temperature and dynamics

F. M. Flasar, R. E. Samuelson & B. J. Conrath

Laboratory for Extraterrestrial Physics, NASA/Goddard Space Flight Center, Greenbelt, Maryland 20771, USA

In the lower atmosphere of Titan IR brightness temperatures exhibit meridional contrast ≲3 K. Seasonal variations are absent because of the large radiative time constant. In the upper stratosphere meridional contrasts are ~20 K, consistent with 100 m s^{-1} cyclostrophic zonal winds, and the radiative time constant is short, implying a large seasonal variation in the temperature and wind field. The absence of longitudinal thermal structure implies that zonally symmetric flows effect the meridional transport of heat. A simple model yields meridional velocities ~0.04 cm s^{-1} and vertical eddy viscosities ~10^3 cm^2 s^{-1} in the lower troposphere, and meridional velocities ~5 cm s^{-1} in the upper stratosphere.

COVERAGE of Titan by the IR instrument (IRIS) during the Voyager 1 encounter provided information on the global thermal structure of the satellite and its atmosphere at relatively high spatial resolution. Here we present data obtained in three spectral intervals which sample the lower troposphere and surface, tropopause, and the upper stratosphere. We discuss the meridional and longitudinal thermal structure implied by the data. Finally, we estimate radiative time constants at various levels of Titan's atmosphere and examine a class of dynamical flows which are consistent with the data.

Observations

The data were obtained over a 6-h interval when the spacecraft was within 2×10^5 km of the center of Titan and the instrument field of view was less than one-third of the satellite's 2,570 km radius. The season on Titan was close to northern spring equinox. Three spectral regions have been analysed. In the first, centred at 530 cm^{-1}, the total optical thickness of the atmosphere is $\tau \lesssim 0.6$ (ref. 1). The major contributor to the opacity is pressure-induced absorption of molecular hydrogen from H_2–N_2 collisions. As this effect is confined to a vertical range close to the ground, the 530 cm^{-1} brightness temperature should be close to the actual surface temperature. Brightness temperatures near 200 cm^{-1} correspond approximately to the tropopause temperature[1]. The 200 cm^{-1} opacity has been inferred to be fairly large ($\tau \gtrsim 3$), confined mainly to clouds, and constrained to a vertical range over which the atmosphere is essentially isothermal. Finally, the 1,304 cm^{-1} ν_4 Q-branch of methane is associated with emission from the ~0.3 mbar pressure level.

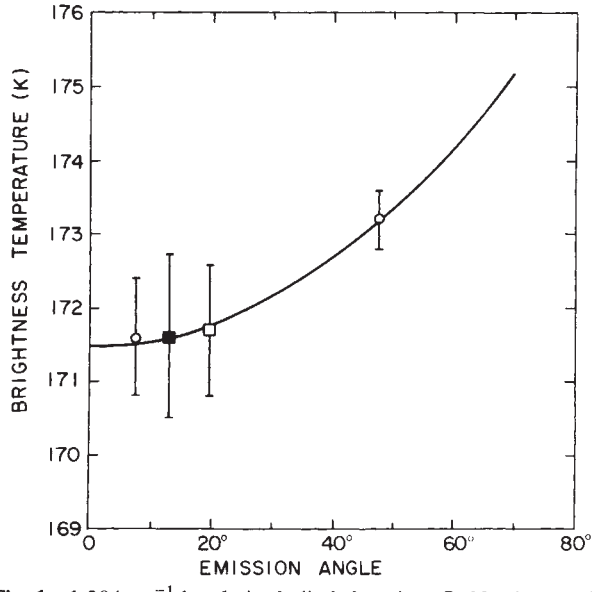

Fig. 1 1,304 cm^{-1} low latitude limb function. ○, Northern latitude daytime data; □, southern daytime data; ■, southern nighttime data. Error bars include uncertainties due to noise and calibration.

0028-0836/81/340693—06$01.00

Table 1 1,304–1,260 cm^{-1} brightness temperature differences

Latitude	Emission angle	T_B(1,304)	T_B(1,260)	δT_B(K)
−55.0°	50.5°	169.8±0.7	153.7±1.7	16.1±1.9
+7.5°	47.5°	173.2±0.4	156.7±1.3	16.5±1.4
+52.6°	50.5°	168.1±0.9	149.1±2.1	19.0±2.3

Vertical temperature gradients produce an emission angle dependence in the observed radiance, which must be removed to infer the horizontal structure in atmospheric temperature. We have therefore normalized the data in each wavenumber region to a common emission angle. Corrections at 200 cm^{-1} and 530 cm^{-1} were determined from a spectral limb function derived from data[1] restricted to the latitude range 0–15° N. These corrections have been applied to the data at all latitudes, even though there seems to be a subtle but real meridional change in opacity across the equator. There is no rigorous justification for doing this; however, as the corrections tend to be small (≤0.8 K at 200 cm^{-1} and ≤0.3 K at 530 cm^{-1}) any corresponding systematic error should also be small.

The larger emission angle corrections at 1,304 cm^{-1} are more reliable. Horizontal opacity inhomogeneities (due to clouds, for example) are not as likely near the 0.3 mbar level as they are at lower altitudes. Moreover, the difference between the brightness temperatures at 1,260 cm^{-1} and 1,304 cm^{-1}, divided by the difference in altitudes at which the respective CH_4 weighting functions peak, gives a crude approximation of dT/dz at each geographical location. Figure 1 depicts the emission angle corrections derived for low latitudes. Table 1 shows the spectral brightness temperature differences $\delta T_B = T_B(1,304) - T_B(1,260)$ at three widely separate latitudes where enough spectra are available for sufficient signal at 1,260 cm^{-1}. The emission angles are very similar, and the values of δT_B are identical to within the noise of the data. As CH_4 should be uniformly mixed at these levels, the altitude difference between weighting functions should be independent of geographical location. Thus the emission angle corrections derived for low latitudes should also be valid at high latitudes.

Other uncertainties and corrections exist. The statistical uncertainty due to noise was generally about ±1 K at 1,304 cm^{-1}; at 200 cm^{-1} and 530 cm^{-1} it was smaller, ±0.1 K, because it was possible to average over fairly wide spectral intervals (60–80 cm^{-1}) and because the IRIS signal-to-noise ratio was higher at these wavenumbers. Finally, all nightside data were corrected for a time-dependent calibration drift of the instrument. This drift occurred principally from the heating of the secondary mirror of the instrument which occurred when it became exposed to direct sunlight. The uncertainty in these calibration corrections is <0.1 K at 1,304 cm^{-1} and ~0.4 K and 0.5 K at 200 cm^{-1} and 530 cm^{-1}, respectively.

Results

The data have been examined for evidence of longitudinal structure. At several latitudes there were day/night observations separated by ~180° in longitude. At low latitudes longitudinal coverage was more extensive, though not complete; over limited spans of longitude, scales down to 30° could be resolved. In general fewer spectra could be averaged in this analysis than in the study of meridional structure, and the uncertainties exceeded the formal errors quoted above. Within these uncertainties, no longitudinal or hour angle dependence of brightness temperature was discernible. Reasonable upper limits on temperature variation are 1 K at 200 cm^{-1} and 530 cm^{-1} and 3 K at 1,304 cm^{-1}.

Meridional variations in temperature are better defined. Table 2 summarizes all the data used. The number of spectra used in obtaining the mean brightness temperatures T_B are listed and the mean latitude and emission angle α of the data set are given. Also indicated is the emission angle correction $\Delta T_B(\alpha)$ required to normalize T_B to $\alpha = 52.7°$. Finally, brightness temperatures corrected for emission angle are listed. The associated uncertainties are the sum of uncertainties due to noise, emission angle corrections, and nightside calibration corrections. Because the first represents a random error while the last two are systematic, we considered the sum of their magnitudes rather than a vector sum in estimating the total error. The corrected brightness temperatures are also shown in Fig. 2. Vertical bars represent the uncertainties listed in Table 2, while horizontal bars indicate the latitude range, defined by the centres of the relevant fields of view, over which the data set comprising each point extend.

The meridional variation in brightness temperature at 200 cm^{-1} is small. Brightness temperatures in the northern hemisphere are ~1 K higher than those at southern latitudes; a sharp transition occurs near 10° S. The meridional contrast in atmospheric temperature must also be small. The principal source of opacity at 200 cm^{-1} has been inferred to be a system of methane clouds, situated mainly at or just below the tropopause (~100 mbar) and ~3 in total optical thickness over northern low latitudes. No configuration of clouds with these opacities could mask meridional contrasts larger than a few degrees, as the temperature lapse rate is small near the tropopause. The small difference in brightness temperature between northern and southern latitudes may be an opacity rather than a thermal effect. As the abundance of stratospheric methane is controlled by saturation just below the tropopause[1,2], the methane cloud system will not extend very far into the stratosphere. An increase to $\tau \sim 4$ over southern latitudes would easily account for the ~1 K brightness temperature reduction. The correlation between our data and the enhanced visual brightness in the southern hemisphere found by Smith *et al.*[3] also suggests methane clouds. The opacity 'boundary' at ~10° S latitude seems to correlate fairly well with that discovered by Smith *et al.*[3] within about ±5° of the equator.

At 530 cm^{-1}, where the effective emission level is close to the ground[1], there is a real temperature variation with latitude. Pressure-induced H_2 absorption is the major opacity source while that from clouds is relatively small, implying that the effective emission level is perhaps ~1,500 mbar. The thermal variation with latitude is roughly symmetric about the equator. At low latitudes the daytime temperatures, which have smaller errors, are slightly warmer in the north than in the south. This may very well reflect a higher atmospheric opacity in the south, possibly from clouds at higher altitudes. This would be consistent with the north/south opacity difference inferred at 200 cm^{-1}. When extrapolated, the data suggest a total equator-to-pole surface temperature variation of about 3 K.

In contrast the meridional variation of the 1,304 cm^{-1}

Table 2 200, 530, and 1,304 cm^{-1} latitudinal temperature distributions

Day/night	No. spectra	Latitude (deg) 200 cm^{-1} / 530 cm^{-1}	Latitude (deg) 1,304 cm^{-1}	Emission angle α (deg) 200 cm^{-1} / 530 cm^{-1}	Emission angle α (deg) 1,304 cm^{-1}	T_B(K) 200 cm^{-1}	T_B(K) 530 cm^{-1}	T_B(K) 1,304 cm^{-1}	$\Delta T_B(\alpha)$ 200 cm^{-1}	$\Delta T_B(\alpha)$ 530 cm^{-1}	$\Delta T_B(\alpha)$ 1,304 cm^{-1}	T_B(corr) 200 cm^{-1}	T_B(corr) 530 cm^{-1}	T_B(corr) 1,304 cm^{-1}
N	13	−59.6	−55.0	54.6	50.5	72.8	91.3	169.8	+0.2	0	−0.2	73.0±0.5	91.3±0.6	169.6±0.7
N	8	−48.3	−45.0	45.8	42.0	73.3	91.3	173.5	−0.1	−0.1	+0.4	73.2±0.5	91.2±0.6	173.9±0.8
D	4	−29.6	−27.5	47.1	43.5	73.1	92.2	174.6	−0.5±0.2	−0.1	+0.4	72.6±0.3	92.1±0.2	175.0±1.0
D	6	−10.0	−9.5	21.0	19.5	74.1	92.8	171.7	−0.6±0.1	−0.3	+1.4	73.5±0.2	92.5±0.1	173.1±0.9
N	5	−8.7	−8.7	13.7	12.8	74.8	92.6	171.6	−0.7	−0.4	+1.6	74.1±0.5	92.2±0.6	173.2±1.1
D	29	+7.2	+7.5	52.7	47.5	74.0	93.1	173.2	0	0	0	74.0±0	93.1±0	173.2±0.4
D	10	+8.3	+8.4	7.3	7.3	74.8	93.5	171.6	−0.8	−0.4	+1.6	74.0±0	93.1±0.1	173.2±0.8
D	5	+33.9	+32.0	30.9	29.8	74.5	93.1	171.6	−0.5±0.2	−0.3	+1.0	74.0±0.2	92.8±0.1	172.6±1.1
N	6	+35.7	+33.5	45.8	42.0	74.2	91.9	171.2	−0.2±0.1	−0.1	+0.4	74.0±0.6	91.8±0.6	171.6±1.1
D	10	+57.1	+52.6	55.0	50.5	73.6	91.3	168.3	+0.1	0	−0.2	73.7±0.1	91.3±0.1	168.1±0.9
D	6	+67.4	+61.4	66.9	59.2	73.7	90.8	164.8	+0.7±0.4	+0.3±0.1	−1.0	74.4±0.5	91.1±0.3	163.8±1.4

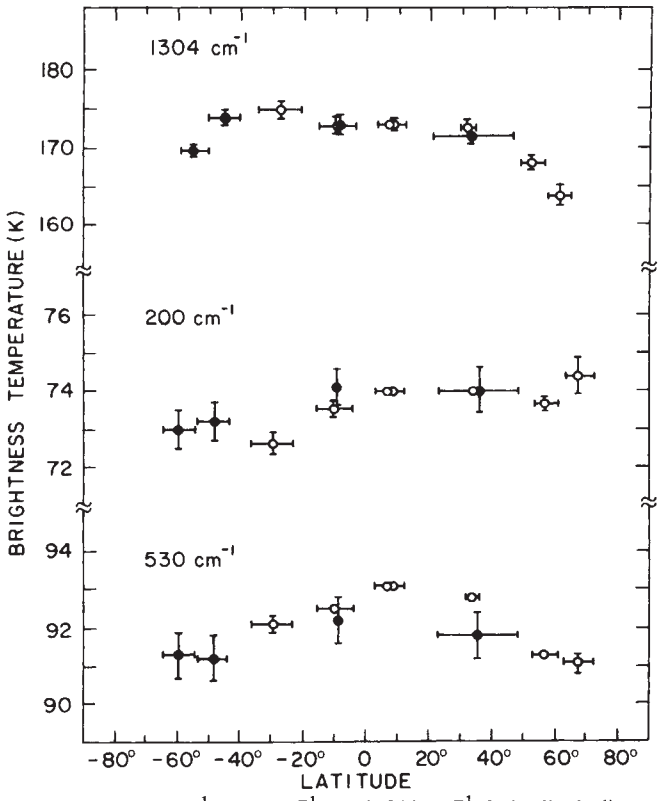

Fig. 2 1,304 cm^{-1}, 530 cm^{-1}, and 200 cm^{-1} latitudinal distributions of brightness temperature. The 1,304 cm^{-1} distribution is normalized to an emission angle $\alpha = 47.5°$, while the other two are normalised to $\alpha = 52.7°$. ○, Daytime data; ●, night-time data. Vertical bars include uncertainties due to noise, calibration, and emission angle corrections. Horizontal bars denote the latitude range over which data comprising each point extend.

brightness temperature is much larger. Although the extrapolation is large, the poles are apparently 20 K colder than the equatorial region. There is a hemispheric asymmetry, the southern hemisphere being 3 K warmer at mid latitudes than the northern hemisphere. The structure is probably thermal in origin with little or no contribution from meridional opacity variations along constant pressure surfaces. After correcting for an emission angle of 47.5° (to which the data are normalized) the effective emission angle is less than that for the lower wavenumbers ($\alpha = 52.7°$), because of its functional dependence on altitude in an extended spherical atmosphere. This also accounts for the slight compression of the 1,304 cm^{-1} data along the latitude axis relative to the data at the lower wavenumbers.

Discussion

The observed thermal structure of an atmosphere represents the radiative–dynamical response to an imposed thermal driving, such as solar heating. An important measure of the inertia of an atmosphere to this driving is its radiative relaxation, or response time τ_R, (ref. 4). Smith *et al.*[3] have estimated the radiative response time of Titan's lower troposphere to be $\sim 4 \times 10^9$ s, or 140 yr. This is much longer than a season on Titan. If $\Omega_s =$ 2π/(Saturn's orbital period $\simeq$29.5 yr), $\Omega_s \tau_R \simeq 30$. Such a large value implies almost no seasonal variation in temperature. At each latitude, temperatures should respond to the annual mean insolation which is symmetric about the equator. The symmetry evident in the brightness temperatures at 530 cm^{-1} is consistent with this.

Estimates of the radiative response time near the tropopause, to which the 200 cm^{-1} brightness temperatures in Fig. 2 pertain, are not presently feasible. Most of the tropopause emission is at wavenumbers below 200 cm^{-1} for which we have no data. The low meridional contrast in brightness temperature at 200 cm^{-1} suggests little seasonal variation in temperature. Either the radiative time constant at the tropopause is large, $\Omega_s \tau_R \gg 1$, or the heating at this level is predominantly from absorption of radiation emitted lower in the atmosphere where τ_R is large and seasonal effects are small.

Radiative time constants can be estimated for Titan's stratosphere. The contribution from gaseous emission is taken into account using the formulation of Harshvardhan and Cess[5], which assumes direct cooling to space. The cooling rate N (s^{-1}) at a pressure level P is

$$N = -\frac{\pi g}{C_p P} \Delta\nu \frac{\partial \tau_{\Delta\nu}}{\partial \ln P} \frac{dB_{\nu_0}}{dT} \quad (1)$$

where $\tau_{\Delta\nu}$ is the transmittance averaged over a wavenumber interval $\Delta\nu$ (cm^{-1}), B_{ν_0} is the Planck function (erg s^{-1} cm^{-1} sr^{-1}) at ν_0, g is the local gravitational acceleration, T is temperature, and C_p is the specific heat. Transmittances have been obtained from a line by line spectral integration for CH_4 ($\nu_0 = 1{,}304$ cm^{-1}, $\Delta\nu = 200$ cm^{-1}), C_2H_6 ($\nu_0 \simeq 820$ cm^{-1}, $\Delta\nu = 85$ cm^{-1}), and C_2H_2 ($\nu_0 \simeq 729$ cm^{-1}, $\Delta\nu = 95$ cm^{-1}) (V. Kunde personal communication). Each gas was assumed to be distributed uniformly with height in the stratosphere with an abundance inferred from its observed IR emission[2]. Radiative response times were obtained by summing over the three species (Table 3).

Radiative response times in the upper stratosphere (0.3 mbar $< P <$ 10 mbar) are short relative to Titan's seasons but still long compared with its day. Note that the times are smaller than the preliminary estimates given by Hanel *et al.*[2]. The longer radiative time constants in the lower stratosphere mainly result from the decrease in T (and hence dB_{ν_0}/dT) with depth in this region[2,6]. The assumption of a uniform vertical distribution is valid only if there is rapid vertical mixing. If C_2H_6 and C_2H_2 are end products of the photo-dissociation of CH_4 at high levels of the atmosphere ($P \ll 0.1$ mbar)[7], less efficient mixing would imply that the concentrations of C_2H_6 and C_2H_2 increase with height. This would effect a decrease in response times in the upper stratosphere, and an increase at lower levels, relative to those listed in Table 3.

It has been concluded[1] that some of the emission at 200–600 cm^{-1} originates in the stratosphere, probably from aerosols. As the stratosphere is optically thin in this wavenumber range, the level of emission cannot be unambiguously determined. However, the deduced wavelength dependence of the aerosol emissivity is more like that expected for small particles if the emission is from the lower stratosphere ($P \sim 10$–30 mbar). If the aerosol emission is confined to a slab one scale height thick with emissivity ε_ν and temperature T, the radiative response time of the slab is given by

$$\tau_R^{-1} \simeq \frac{2\pi g}{C_p P} \int_{200\ cm^{-1}}^{600\ cm^{-1}} \varepsilon_\nu \frac{dB_\nu}{dT} d\nu \quad (2)$$

Table 3 lists τ_R at two pressure levels. The aerosol component reduces τ_R significantly below that computed for gaseous emission alone. This suggests that aerosols are the major source of cooling in the lower stratosphere.

In the upper stratosphere near 1 mbar $\Omega_s \tau_R \ll 1$, and there should be no lag in the thermal response. As only a small fraction of incident solar radiation is absorbed at higher altitudes, the meridional distribution of solar heating and temperature at solstice will be flat in the summer hemisphere, with a slight maximum at the pole, provided that the sources of thermal and solar opacity are uniformly distributed with latitude[8,9]. The winter hemisphere will be colder with sharper gradients in temperature. At the equinoxes the temperature distribution

Table 3 Radiative response times in Titan's stratosphere

		Gaseous radiative cooling rate N(s^{-1})			τ_R(s)		$\Omega_s \tau_R$	
P(mbar)	T(K)	CH_4	C_2H_6	C_2H_2	Gas	Aerosol	Gas	Aerosol
0.3	173	2×10^{-8}	3×10^{-8}	2×10^{-8}	2×10^{7}	—	0.1	—
1	170	1×10^{-8}	7×10^{-9}	1×10^{-8}	3×10^{7}	—	0.2	—
10	149	1×10^{-9}	4×10^{-9}	4×10^{-9}	1×10^{8}	4×10^{7}	0.7	0.2
30	104	3×10^{-12}	2×10^{-10}	5×10^{-10}	1×10^{9}	7×10^{7}	9.0	0.5

should be symmetric about the equator, being warmest there and coldest at the poles. The meridional distribution of the 1,304 cm^{-1} brightness temperature at northern spring equinox (Fig. 2) roughly accords with the latter case, but the ~3 K hemispheric asymmetry evident at mid-latitudes is puzzling. Meridional variations in the infrared flux emitted deeper in the atmosphere where $\Omega_s\tau_R \geqslant 1$ cannot explain the asymmetry, as the flux is emitted at lower temperatures and does not contribute significantly to the radiative heating near 1 mbar. A hemispheric asymmetry in opacity is possible. On Earth, for example, seasonal variations in the meridional distribution of ozone account for the seasonal behaviour of stratospheric temperatures[10]. Although variations in aerosols and gaseous absorbers such as C_2H_2 and C_2H_6 are possible on Titan, we cannot unambiguously account for the observed asymmetry.

Figure 3 represents schematically $\Omega_s\tau_R$ with pressure level. Because of the uncertainties in the location of the stratospheric aerosol emission and in the radiative time constant at the tropopause, the transition from $\Omega_s\tau_R \ll 1$ high in the stratosphere to $\Omega_s\tau_R \gg 1$ lower down is not defined very precisely.

The meridional temperature gradients depicted in Fig. 2 imply a zonal thermal wind, u. If the surface drag is sufficiently strong, $u(z=0) \approx 0$, and

$$\frac{u^2(z)}{a}\tan\Lambda + 2\Omega\sin\Lambda\, u(z) = -\frac{1}{a}\int_0^z \frac{g}{T}\partial_\Lambda T\, dz \qquad (3)$$

where Λ is latitude, z is height, $a = 2{,}570$ km is the radius of Titan[6], $\Omega = 4.5\times10^6\ s^{-1}$ is its frequency of rotation, and T is atmospheric temperature. If we assume that the meridional temperature has the form $T(z,\Lambda) = T_0(z) + \Delta T(z)\cos\Lambda$ and $\Delta T = 3$ K throughout the troposphere, then at the tropopause ($z \simeq 60$ km, $P \simeq 100$ mbar) we infer an eastward velocity of $u \simeq 36\ m\ s^{-1}$ at 45° latitude. This is approximately three times the surface rotational speed at Titan's equator. The larger horizontal contrasts in temperature in the stratosphere imply even stronger zonal winds. We assume that the thermal contrast between the equator and pole increases linearly with ln$P$ from 3 K at 100 mbar to 20 K at 0.5 mbar. At 45°, equation (3) yields $u(0.5\ mbar) \simeq 110\ m\ s^{-1}$. The estimate of the stratospheric zonal winds is uncertain insofar as we have no direct knowledge of the meridional temperature structure in the lower stratosphere. Nonetheless, it is hard to avoid the conclusion that there are global cyclostrophic flows ($u/\Omega a \gg 1$) in Titan's atmosphere. The occurrence of such flows in the atmosphere of Venus is already well established[11]. However, unlike Venus, Titan has a large obliquity. The temperatures in its upper stratosphere, where $\Omega_s\tau_R$ is small compared with one, should exhibit a large seasonal variation. From equation (3), we expect a concomitant variation in the zonal winds at high altitudes.

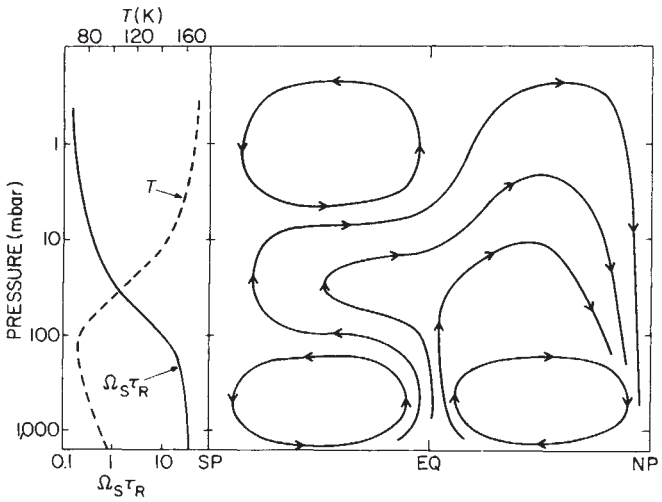

Fig. 3 Schematic diagram of the meridional flow in Titan's atmosphere at northern spring equinox. Mean vertical profiles of temperature and radiative relaxation time are indicated at the left.

Table 4 Radiative and dynamical characteristics of Titan's atmosphere

	$\Delta\theta$ (K)	D (km)	$\delta\theta$ (K)	τ_R (s)	V (cm s^{-1})	a/V (s)	κ ($cm^2\ s^{-1}$)
Lower troposphere ($P \sim 1{,}000$ mbar)	3	28	22	4×10^9	0.04	7×10^9	10^3
Upper stratosphere ($P \sim 1$ mbar)	20	42	60	3×10^7	5	6×10^7	—

The condition that $u(0)$ be small compared with the zonal winds at higher levels requires that the time for surface drag to deplete the relative zonal momentum of the atmosphere be small compared with the other dynamical time scales of the problem[12]. We assume a surface stress of the form $C_D u(0)^2$, where $C_D \simeq 3\times10^{-3}$ is a dimensionless drag coefficient[13]. For vertical scales ($D \simeq 28$ km) and zonal velocities characteristic of the lower troposphere, the surface drag time is only[12] $D/C_D u(D) \sim 10^6$ s. We will show that the meridional turnover time is much larger, $\sim 10^{10}$ s (Table 4).

The long radiative time scales in Titan's atmosphere imply that there should be no diurnal response to solar heating and this is consistent with the absence of discernible longitudinal structure in the data. The absence of this structure, however, also implies that baroclinic eddies do not have an important role in Titan's atmosphere. Previously, Leovy and Pollack[13] concluded that baroclinic eddies are probably not effective in transporting heat on Titan. Assuming a vertical structure close to adiabatic, they found that the preferred scale of the eddies exceeded the radius of the satellite. Voyager observations, however, indicate a temperature lapse rate which is much more stable[2,6]. This increases the preferred scale of the eddies and strengthens Leovy and Pollack's original conclusion that zonally symmetric flow constitutes the favoured mode of meridional heat transport.

Following Leovy and Pollack[13], we consider zonally symmetric, thermodynamically direct, meridional circulations of horizontal dimension $\sim a$. There are several reasons for considering only thermally direct flows. First, the thermal contrasts forced by differential solar heating will induce a meridional transport of heat which will reduce these contrasts for the atmosphere as a whole. Second, the observed temperatures in the lower troposphere and upper stratosphere, the two regions of the atmosphere which we can treat quantitatively, are consistent with thermally direct flows. The global temperature contrasts are in the same sense as those which would obtain from purely radiative effects but reduced in magnitude. Finally, a thermally direct circulation is the simplest, and allows straightforward calculation, provided that the meridional contrasts in temperature and radiative time constants are known. Given the gaps in our knowledge of Titan's atmosphere, consideration of more complex flows is unwarranted.

We use here the Boussinesq approximation, although this limitation does not affect our conclusions. Consider an idealized meridional cell confined to altitudes z_0 and $z_0 + D$, and latitudes 0 and $\pi/2$. Let the symbol $\delta(\ )$ denote the vertical contrast in a given quantity ($\delta(\ ) = (\ )_{z=z_0+D} - (\ )_{z=z_0}$) averaged over latitudes 0, $\pi/2$; Let $\Delta(\ )$ denote the contrast over latitude ($\Delta(\ ) = (\ )_{\Lambda=0} - (\ )_{\Lambda=\pi/2}$) averaged over the depth D. The thermodynamic heat equation can be cast into the form[24]:

$$\partial_t\Delta\theta + \frac{V}{a}\delta\theta \sim \frac{\Delta\theta_e - \Delta\theta}{\tau_R} \qquad (4)$$

where θ denotes potential temperature, and factors of the order of unity have been neglected. The term on the right-hand side represents radiative heating and cooling in terms of a linear relaxation back to the radiative equilibrium state, θ_e. The second term on the left-hand side represents the poleward transport of sensible heat and potential energy by the meridional cell. V is a mass-weighted meridional velocity averaged over the upper or lower leg of the cell. When $\Delta\theta > 0$, there is upwelling at low latitudes and poleward motion in the upper leg of the cell. The condition $\delta\theta > 0$ ensures that net transport of energy is poleward[14], and the circulation acts to reduce $\Delta\theta$ ($\partial_t\Delta\theta < 0$). We will use equation (4) to estimate the magnitude of the meridional circulation at various altitudes in Titan's atmosphere.

In the troposphere ($z_0 = 0$) the long radiative response time and absence of detectable seasonal variation imply a steady circulation, $\partial_t \equiv 0$, symmetric about the equator. As the lower troposphere contains most of the atmospheric mass, we choose D = 1.5 scale heights ≈28 km. Over this interval $\delta\theta \simeq 22$ K (refs 2, 4). As the inclination of Titan's rotational axis to the ecliptic is presumably 27°, the annual mean insolation of the polar regions is half that at equatorial latitudes[15]. A crude estimate of $\Delta\theta_e$ follows from

$$\left(\frac{\theta_e(\Lambda = 0)}{\theta_e\left(\Lambda = \frac{\pi}{2}\right)}\right)^4 \sim 2.$$

With $\theta_e(\Lambda = 0) \simeq 95$ K, $\Delta\theta_e \simeq 15$ K. The temperature contrast observed in the troposphere (Fig. 2) is much less, $\Delta\theta \sim 3$ K. With these estimates, equation (4) implies $V \sim 0.04$ cm s^{-1}, equivalent to a dynamical turnover time, a/V, $\sim 7 \times 10^9$ s ~200 yr (Table 4).

Two potentially important transports have been neglected in this discussion of the Hadley circulation. The first is the equatorward transport by the circulation of latent heat associated with methane condensation. The second is the poleward transport of sensible heat by deep reservoirs of liquid methane which may exist on the surface of Titan. The magnitude of these transports relative to the atmospheric transport of sensible heat and potential energy is difficult to estimate. On Earth, where water is the condensate, they are all comparable, at least over those latitudes where the Hadley circulation dominates[16]. In this complex situation, the net poleward transport of energy on Earth is still comparable to the atmospheric transport of sensible heat and potential energy alone. This suggests that our estimates remain correct to order of magnitude.

In the upper stratosphere the radiative response times are short. Since $\partial_t \sim \Omega_S \ll \tau_R^{-1}$, the time derivative in equation (4) can be neglected: the upper stratosphere is in radiative–dynamical balance with the current value of the seasonal forcing. For the estimate we assume a vertical scale of one scale height. At the equinoxes, radiative equilibrium implies $\Delta\theta_e \sim 10^2$ K. Using the thermal contrast $\Delta\theta \sim 20$ K inferred from the 1,304 cm^{-1} data, we estimate $V \sim 5$ cm s^{-1} (Table 4).

The transition from $\Omega_s\tau_R \ll 1$ in the upper stratosphere to $\Omega_s\tau_R \gg 1$ occurs in the lower stratosphere and tropopause region, as noted earlier. In the lower stratosphere the thermal response will lag the solar forcing; if $\Omega_s\tau_R \sim 3$ the lag is close to its asymptotic value of one season[17]. At the northern spring equinox, temperatures within the lower stratosphere should be warmer in the southern hemisphere than in the north. Such a thermal asymmetry would induce a pole to pole circulation with rising motion in the southern hemisphere. If such a circulation penetrated into the tropopause region, where the seasonally varying radiative heating is probably smaller, adiabatic cooling could conceivably be sufficiently strong to produce lower temperatures and enhanced condensation in the southern hemisphere, as suggested by the observations at 200 cm^{-1}. On the basis of the visible hemispheric asymmetry, Smith *et al.*[3] suggested such a circulation for the lower troposphere. However, the magnitudes of radiative response times (Tables 3 and 4) and the global hemispheric symmetry observed at 530 cm^{-1} (Fig. 2) suggest that such a cross equatorial circulation is more likely situated in the lower stratosphere and tropopause region.

Figure 3 illustrates one possible model of the meridional flow in Titan's troposphere and stratosphere at northern spring equinox; it assumes a uniform distribution of opacity with latitude. The topology indicated has to be speculative, because we lack sufficient information on the vertical structure of the meridional contrasts in temperature. This cannot be achieved until the vertical distribution of IR opacity is known, particularly in the lower stratosphere and troposphere. Note, however, that the vertical mass flux in the ascending leg of the meridional cell in the upper stratosphere is 0.1 that in the lower troposphere. Thus the streamlines in the stratospheric circulation possibly close in the lower troposphere, as apparently occurs on Earth[18,19].

Although eddy transport of heat may not be important on Titan, eddies are crucial in the maintenance of its zonal momentum. The zonal velocity of 36 m s^{-1} at 45° latitude, computed earlier, corresponds to an angular momentum per unit mass of $3\Omega a^2$. In the upper stratosphere the corresponding angular momentum per unit mass is $2\frac{1}{2}$ times larger. The angular momentum per unit mass in a zonally symmetric circulation controlled by down-gradient angular momentum fluxes is limited to Ωa^2 (refs 12, 20). Atmospheres with excess angular momentum therefore require other transport mechanisms, such as lateral mixing of vorticity or angular velocity by barotropic eddies[21–23]. Upward transport of zonal momentum by vertically propagating waves is another possibility[23], although the lack of longitudinal structure in the observations precludes most conceivable planetary-scale waves on Titan.

The vertical transport of angular momentum by a zonally symmetric meridional cell must be balanced in a steady state by vertical eddy transport. The angular momentum equation, averaged over a horizontal surface from $\Lambda = 0$ to $\pi/2$, is [21]

$$\partial_t \int_0^{\pi/2} d\Lambda \cos\Lambda M + \int_0^{\pi/2} d\Lambda \cos\Lambda \partial_z(WM) = \int_0^{\pi/2} d\Lambda \cos\Lambda \partial_z(\kappa \partial_z M) \quad (5)$$

In equation (5) M denotes the angular momentum per unit mass, W is vertical velocity, and κ is an eddy diffusion coefficient for vertical mixing of momentum. We have assumed the horizontal fluxes to be zero at $\Lambda = 0$, $\pi/2$. Consider the lower troposphere which contains the bulk of the atmospheric mass and momentum; here the flow is steady ($\partial_t \equiv 0$). The requirement that there be no net exchange of angular momentum between the lower troposphere and surface implies that the vertical flux of angular momentum across a horizontal surface vanish, permitting equation (5) to be written as

$$W\Delta M \sim 2\frac{\kappa\,\delta M}{D} \quad (6)$$

The quantities ΔM and δM denote, respectively, the horizontal and vertical contrasts in angular momentum. An atmosphere with $\partial_z u > 0 (\delta M > 0)$ requires that the equatorial angular momentum exceed that at polar latitudes ($\Delta M > 0$)[21]. Knowing the meridional velocities from thermodynamic considerations (Table 4) permits an estimate of κ. Since $u(D) \sim \Omega a$ and $u(0) \simeq 0$, in the lower atmosphere of Titan $\delta M \sim \langle M \rangle$, a tropospheric average. A Hadley cell which conserves angular momentum in its (upper) poleward branch will have $\Delta M \cong 0$. On the other hand, if eddy mixing of vorticity or angular velocity across latitudes is sufficiently vigorous, $\Delta M \sim \langle M \rangle$. Thus we expect $\Delta M/\delta M \leqslant 1$ and from equation (6)

$$\kappa \leqslant DW \sim \frac{D^2}{a} V \sim 10^3 \text{ cm}^2 \text{ s}^{-1}$$

From analogous considerations, Gierasch[21] inferred a low value of vertical viscosity in the atmosphere of Venus, $\kappa \sim 10^4$ cm^{-1}. Note that equation (6), with the added condition $\Delta M/\delta M \leqslant 1$, requires that the time for diffusion of momentum vertically through the troposphere, D^2/κ, not exceed the dynamic turnover time, a/V.

Leovy and Pollack[13] proposed a symmetric model of Titan's tropospheric circulation and deduced meridional velocities much larger and thermal contrasts smaller than those presented here. Although their model differs from ours in several specific aspects, the most important difference lies in their treatment of internal friction. In not distinguishing between $u(0)$ and $u(D)$, they in effect assumed a Rayleigh friction drag in the angular momentum equation. They therefore implicitly assumed $\kappa \sim C_D u(D) D \sim 10^7$ cm^2 s^{-1}, well in excess of our derived upper limit. From equation (6) this resulted in larger meridional velocities, $V \sim 1$ m s^{-1}, and smaller thermal contrasts. The

anticipated seasonal variation in the zonal wind field of the stratosphere presents a more complex situation, and we will not attempt to analyse the requisite angular momentum transports.

Conclusions

IR brightness temperature at 200 cm^{-1}, 530 cm^{-1}, and 1,304 cm^{-1} exhibit small meridional contrasts ($\lesssim$3 K) in the troposphere and tropopause region and larger contrasts ($\sim$20 K) in the upper stratosphere. Radiative relaxation times estimated for the troposphere and stratosphere are large compared with the length of Titan's day. In the lower troposphere they are also large compared with the length of a season, $\Omega_s\tau_R \gg 1$, implying a lack of seasonal variation in temperature. In the upper stratosphere, $\Omega_s\tau_R \ll 1$, and seasonal variations in temperature should be large. The location of the transition region, where $\Omega_s\tau_R \simeq 1$, is not well determined.

The absence of detectable longitudinal structure in the observations suggests that baroclinic waves and eddies are absent in Titan's atmosphere. Zonally symmetric flows are the preferred mode of meridional heat transport and thermally driven planetary-scale circulations yield characteristic meridional velocities of 0.04 cm s^{-1} in the lower troposphere and 5 cm s^{-1} in the upper stratosphere.

The observed meridional temperature contrasts imply zonal winds which are cyclostrophic, reaching $\sim$100 m s^{-1} in the upper stratosphere. The anticipated seasonal variation in the stratospheric temperature field implies a concomitant variation in the zonal winds at high altitudes. The inferred cyclostrophic flow has an angular momentum per unit mass which, at least in the stratosphere, greatly exceeds Ωa^2. In the lower troposphere, an assumed balance in the vertical transport of angular momentum by zonally symmetric meridional flow and down gradient diffusion implies a vertical viscosity of only 10^3 cm^2 s^{-1}.

We thank V. G. Kunde for gaseous transmittance tables for Titan's stratosphere, W. C. Maguire for helpful discussions, also M. E. Geller, P. J. Gierasch, C. B. Leovy and R. A. Hanel for their critical reading of the manuscript.

Received 18 June; accepted 20 July 1981.

1. Samuelson, R. E., Hanel, R. A., Kunde, V. G. & Maguire, W. A. *Nature* **292**, 688–693 (1981).
2. Hanel, R. *et al. Science* **212**, 192–200 (1981).
3. Smith, B. A. *et al. Science* **212**, 162–190 (1981).
4. Gierasch, P. J., Goody, R. M. & Stone, P. H. *Geophys. Fluid Dyn.* **1**, 1–18 (1970).
5. Harshvardhan & Cess, R. D. *Tellus* **28**, 1–9 (1976).
6. Tyler, G. *et al. Science* **212**, 201–206 (1981).
7. Strobel, D. F. in *Atmospheres of Earth and the Planets* (ed. McCormac, B. M.) 401–408 (Reidel, Dordrecht, 1975).
8. Hess, S. L. *Introduction to Theoretical Meteorology* (Holt, Rinehart and Winston, New York, 1959).
9. Carlson, B. E., Caldwell, J. & Cess, R. D. *J. atmos. Sci.* **37**, 1883–1885 (1980).
10. Prabhakara, C., Rodgers, E. B., Conrath, B. J., Hanel, R. A. & Kunde, V. G. *J. geophys. Res.* **81**, 6391–6399 (1976).
11. Schubert, G. *et al. J. geophys. Res.* **85**, 8007–8025 (1980).
12. Held, I. M. & Hou, A. Y. *J. atmos. Sci.* **32**, 1038–1044 (1975).
13. Leovy, C. B. & Pollack, J. B. *Icarus* **19**, 195–201 (1973).
14. Stone, P. *J. atmos. Sci.* **32**, 1005–1016 (1975).
15. Brinkman, A. W. & McGregor, J. *Icarus* **38**, 479–482 (1979).
16. Lorenz, E. N. *The Nature and Theory of the General Circulation of the Atmosphere* World Meteorological Organization (1967).
17. Cess, R. D. & Caldwell, J. *Icarus* **38**, 349–357 (1979).
18. Geller, M. A. *J. atmos. terr. Phys.* **41**, 683–705 (1979).
19. Dunkerton, T. *J. atmos. Sci.* **35**, 2325–2333 (1978).
20. Schneider, E. K. *J. atmos. Sci.* **34**, 280–296 (1977).
21. Gierasch, P. J. *J. atmos. Sci.* **32**, 1038–1044 (1975).
22. Rossow, W. B. & Williams, G. P. *J. atmos. Sci.* **36**, 377–389 (1979).
23. Leovy, C. B. *J. atmos. Sci.* **30**, 1218–1220 (1973).
24. Stone, P. H. *J. atmos. Sci.* **31**, 1681–1690 (1974).

Implications of Titan's north–south brightness asymmetry

Lawrence A. Sromovsky*, Verner E. Suomi*, James B. Pollack†, Robert J. Krauss*, Sanjay S. Limaye*, Tobias Owen‡, Henry E. Revercomb* & Carl Sagan§

* Space Science and Engineering Center, University of Wisconsin-Madison, Madison, Wisconsin 53706, USA
† NASA Ames Research Center, Moffett Field, California 94035, USA
‡ Department of Earth and Space Sciences, Suny at Stony Brook, Stony Brook, New York 11790, USA
§ Laboratory for Planetary Studies, Cornell University, Ithaca, New York 14853, USA

Voyager 1 *images of Titan, when normalized to remove limb darkening, reveal an axially symmetric brightness pattern with significant north–south asymmetry. This interhemispheric contrast seems to be a response to seasonal solar heating variations resulting from Titan's inclined spin axis. The contrast significantly lags the solar forcing, indicating that its production involves the atmosphere well below the unit optical depth level. The contrast has a significant effect on Titan's disk-integrated brightness as seen from Earth, and probably accounts for most of the observed long term variation, with solar UV variations accounting for the remainder.*

EARTH-based observations[1,2] show that between 1972 and 1976 Titan's disk-integrated brightness increased by $\sim$9% in the blue (b) and $\sim$5.5% in the yellow (y) to a maximum during 1976–77, and decreased through 1978. This variation and a similar but smaller variation in Neptune's brightness can be correlated with the solar cycle[2,3], suggesting solar variability as the common cause. As photochemical reactions are thought to produce the submicrometre aerosols in both atmospheres, we expect the variation in solar UV output during the solar cycle[4,5] to affect the amount or physical properties of the aerosols. Pollack *et al.*[6] showed that Titan's brightness changes during 1972–76 could be produced by changes in mean particle size, visible absorption coefficient, or optical depth, and that the fractional decrease in the particle production rate required to explain the increase in albedo was roughly consistent with the estimated fractional change in solar UV output.

A new mechanism for explaining at least part of the Earth based photometry of Titan is suggested by the Voyager 1 observations of November 1980 that showed Titan to be shrouded in an apparently unbroken cloud cover with several large-scale zonal features and a surprising north–south asymmetry in brightness[7]. As Titan's spin axis is inclined 27° to the ecliptic (assuming Titan is tidally locked to Saturn), the angle between Titan's axis and the line of sight to the Earth varies during Saturn's (and Titan's) 29.5-yr orbit around the Sun. The apparent tipping motion, combined with the brightness asymmetry could result in a long-term periodic variation of Titan's disk-integrated brightness. If the brightness asymmetry also varies in response to seasonal changes in solar heating of the deepest layers of the atmosphere[7], then the contrast would follow the seasonal heating asymmetry with a phase shift of nearly a full season and would reach an extreme value near Titan's equinoxes (near the time of the Voyager 1 encounter). Using a highly simplified model to combine the effects of the suggested seasonal changes in contrast and the time-dependent viewing conditions, the predicted brightness variation is found

0028-0836/81/340698—05$01.00